Chemical Engineering Journal 480 (2024) 148045

Contents lists available at ScienceDirect

Chemical Engineering Journal

journal homepage: www.elsevier.com/locate/cej

A layered/spinel heterostructured cathode for Li-ion batteries prepared by ultrafast Joule heating

Wei Zhu, Hai Su, Panxing Bai, Zhenfei Li, Jingchao Zhang, Jinfeng Zhang, Mengjie Li, Yanan Chen *, Yunhua Xu *

School of Materials Science and Engineering, Key Laboratory of Advanced Ceramics and Machining Technology (Ministry of Education), and Tianjin Key Laboratory of Composite and Functional Materials, Tianjin University, Tianjin 300072, China

ARTICLE INFO

Keywords:
Li-ion batteries
Layered/spinel heterostructured cathode material
Ultrafast synthesis
Joule heating

ABSTRACT

Spinel $LiMn_2O_4$ is one of the most promising cathode materials due to its low cost, high discharge voltage (~4.0 V), and non-toxicity. However, it suffers from insufficient cycling performance caused by irreversible phase transition and Mn dissolution. In addition, the low synthesis efficiency caused by the long heating time also plagues its application and depletes the cost merits of raw materials. Herein, we report a heterostructured cathode material of electrochemically-inert layered Li_2MnO_3 and active spinel $LiMn_2O_4$ phases, which is synthesized in seconds by ultrafast Joule heating. The heterostructure is rapidly formed as a result of the non-equilibrium process produced by the ultrafast Joule heating rate. The inert layered phase serves as a structure stabilization agent to suppress the structure damage and Mn dissolution, thus promising an excellent electrochemical performance with a high capacity retention of 83 % after 800 cycles at 5C. Our findings provide an efficient design and synthesis strategy for developing high-performance and low-cost cathode materials.

1. Introduction

With the worldwide deployment and rapid development of electric vehicles and renewable energy storage, Li-ion batteries (LIBs) with high energy density, long cycle life, and low cost are highly desired [1–4]. The energy density and cost of LIBs highly depend on cathode materials, which are mainly transition metal compounds, such as $LiMn_2O_4$, $LiFePO_4$, $LiCoO_2$, ternary materials $LiNi_xCo_yMn_zO_2$ ($x + y + z = 1$), and Li-rich layered materials $xLiMO_2 \cdot (1\text{-}x)Li_2MnO_3$ (M = Ni, Mn, and Co) [5–10]. Among them, spinel $LiMn_2O_4$ has received remarkable attention because of its high discharge voltage (~4.0 V) and the three-dimensional diffusion channels of Li^+, as well as the abundance of raw materials, non-toxicity, and low cost [11–14]. However, its practical application is plagued by the energy-consuming synthesis and fast capacity fading.

Many synthesis approaches have been developed to prepare spinel $LiMn_2O_4$, including solid-state reaction, combustion, sol–gel, and co-precipitation methods [15]. All these approaches require a long-time heat treatment with slow heating and cooling processes (at least several hours) in a furnace to form a fine crystal structure, due to the slow reaction kinetics during the slow heating ramp [15–19]. For example, it took up to 8 h at 750 °C to synthesize $LiMn_2O_4$ from the precursors of acetate and carbonate using a precipitation method [17]. Apparently, the long-time heating leads to a high energy consumption, high cost, and low manufacturing efficiency. Although some rapid preparation methods have been reported recently, the resulting $LiMn_2O_4$ shows insufficient cycling performance. For instance, $LiMn_2O_4$ can be synthesized in 6 min using a microwave method, while a low capacity retention of 80 % was delivered after 100 cycles at 0.2 mA / cm^2 [20].

In addition to the preparation process, $LiMn_2O_4$ often suffers from a rapid capacity degradation, which can be attributed to the dissolution of Mn ions caused by the disproportionation reaction of Mn^{3+}, the irreversible phase change, and the decomposition of the electrolyte in a high-voltage region [5,21–24]. Extensive efforts have been made to address these issues, such as element doping, surface modification, and morphology engineering [14,25–37]. Cationic doping is an effective way to reduce the Mn^{3+} content, which can enhance the lattice stability of $LiMn_2O_4$ during cycling. For example, Cai et al. reported an Al-doped spinel $LiMn_2O_4$ cathode material, and found that Al doping can suppress the concentration of Mn^{3+}, resulting in improved electrochemical properties [25]. Similar effects were also reported for other doping cations, such as Li, Mg, and Ni [26–28]. Surface modification is also an

* Corresponding authors.
E-mail addresses: yananchen@tju.edu.cn (Y. Chen), yunhua.xu@tju.edu.cn (Y. Xu).

https://doi.org/10.1016/j.cej.2023.148045
Received 12 July 2023; Received in revised form 8 November 2023; Accepted 10 December 2023
Available online 12 December 2023

efficient strategy to reduce the dissolution of Mn ions and minimize side reactions between electrode and electrolyte. Metal oxides and phosphates were widely used as coating materials of $LiMn_2O_4$ [29–35]. Chen et al synthesized Al_2O_3-coated $LiMn_2O_4$ via an atomic layer deposition method, and obtained improved cycling performance compared with the uncoated $LiMn_2O_4$ [35]. Besides doping and surface coating, morphology also plays an important role in enhancing the electrochemical performance, and nanostructured spinel $LiMn_2O_4$ materials with different morphologies, such as nanotubes, flakes, and nanorods, have been widely investigated [14,36,37]. Although these strategies can improve the electrochemical performance, the preparation process is tedious and time-consuming. Therefore, it is highly desired to efficiently synthesize high-performance $LiMn_2O_4$ cathode materials.

Recently, Joule heating has emerged as an ultrafast material synthesis technique [38–41]. It not only reduces energy consumption and increases production efficiency, but also provides a powerful approach to tune material structures and properties. The high heating/cooling rates (10^5 ℃/s) of Joule heating enable a super-fast reaction dynamics and ultrashort reaction time. In addition, the non-equilibrium nature of Joule heating favors the preparation of heterostructured materials. Li et al synthesized a series of single-phase multi-element oxide nanoparticles as catalysts by using Joule heating. Heterostructure can be formed by adjusting the synthesis temperature, composition, and calcination atmosphere [42]. Compared with the single-phase cathode materials, the heterostructured cathode materials showed improved electrochemical performance as the result of the property and structure complementation of different components. Wang et al introduced a small content of perovskite phase into Ni-rich layered cathode material, in which the pinning effect of the perovskite phase mitigated the lattice strain during the charge–discharge processes, and achieved a superior cycling performance [43].

In this work, a layered Li_2MnO_3 and spinel $LiMn_2O_4$ heterostructured cathode material (LS-LMO) is synthesized in seconds by ultrafast Joule heating. The ultrahigh heating rate of Joule heating provides a non-equilibrium process, enabling a fast hetero-phase formation of LS-LMO. The layered Li_2MnO_3 phase is electrochemically inert below 4.3 V, but acts as a structural stabilizer to the spinel $LiMn_2O_4$ (LMO) during cycling to enhance the structural stability. The resulting heterostructured cathode material demonstrates a superior cycling performance (83 % of capacity retention at 5C after 800 cycles).

2. Experimental

2.1. Synthesis of LMO and LS-LMO

2.1.1. Synthesis of the precursor of LMO

0.1 mol lithium acetate dihydrate (5 wt% excess, 99.9 %, Meryer) and 0.2 mol manganese acetate tetrahydrate (99 %, Heowns) were dissolved in ethanol (80 ml) to make Solution 1. 0.2 mol citric acid monohydrate was dissolved in ethanol (80 ml) to make Solution 2. Then Solution 1 and Solution 2 were titrated to 200 ml ethanol under stirring at 80 °C, and a precipitate was produced. The precipitate was collected and dried at 100 °C.

2.1.2. Synthesis of the precursor of LS-LMO

The precursor of LS-LMO was synthesized using the same procedure as that used for LMO, except that a different molar ratio of Li:Mn = 1.09:1.91 was used.

2.1.3. Joule-heating process

The precursor was placed on a carbon cloth (5.0 cm × 2.5 cm, Taiwan Carbon energy Technology) linked to a current source (MP50100D) in the air atmosphere. Then the precursor was calcined in a two-step process to produce the cathode material, including precalcination (~670 ℃ for ~ 9 s) and calcination (~740 ℃ for ~ 9 s). The temperature was tuned by adjusting the current and voltage and monitored by a laser infrared thermometer (Sanya Kechuang Future Technology).

2.1.4. Conventional furnace process

The precursor was calcined at 450 °C for 5 h and 700 °C for 5 h with a heating rate of of 3 °C/min, respectively, and then naturally cooled to room temperature.

2.2. Materials characterization

X-ray diffraction (XRD) patterns were collected on a D8 Advanced X-ray diffractometer with Cu Kα radiation at 40 kV and 40 mA. Rietveld refinements of the XRD pattern were obtained by using a GSAS code with an EXPGUI interface [44]. Morphology was examined by field emission scanning electron microscope (FSEM, s4800). The X-ray photoelectron spectroscopy (XPS, Axis Supra) was used to analyze the valence state of the element and the surface composition of the material. XPS data were calibrated against the C1s peak at 284.6 eV. The valence states of Mn ions were calculated by the following equation: AOS = 8.956–1.126ΔE (ΔE: the splitting energies between the Mn 3 s peak and its satellite peak). The microstructures of the materials were analyzed by transmission electron microscopy (TEM, JEM-2100F) and aberration corrected TEM (JEM-ARM200F). Inductively coupled plasma optical emission spectrometer (ICP-OES, Agilent 5110) was used to measure the amount of Mn deposited on the Li metal.

2.3. Electrochemical measurements

The electrodes were prepared by mixing LMO or LS-LMO (80 wt%), polyvinylidene fluoride (PVDF, 10 wt%) as the binder, and Super P (10 wt%) as the conductive agent with N-methyl-2-pyrrolidone (NMP) to form a uniform slurry. Then the slurry was cast on carbon-coated aluminum foils and vacuum dried at 100 ℃ for 12 h. Then, the electrodes were cut into circular pieces with a diameter of 9 mm. The mass loading of the active material is ~ 1.5 mg cm^{-2}. CR2032 half cells were assembled in an argon-filled glove box using lithium foils anodes, microporous polypropylene membrane (Celgard 2500) separators, and the electrolyte of 0.8 M LiTFSI and 0.2 M LiDFBOP in FEC and EMC (3:7 by volume). Electrochemical tests were performed on a typical NEWARE battery test station in a voltage window of 3.5–4.3 V at various current densities (1C = 148 mAh g^{-1}). Electrochemical impedance spectroscopy (EIS) measurements were performed on Solartron 1470 Electrochemical Interface with an amplitude of 5 mV and a frequency range of 0.01 Hz to 1 MHz. After one cycle activation at 0.1C, galvanostatic intermittent titration (GITT) measurement was conducted at a constant current density of 0.1C with duration of 10 min and 40 min relaxation in the voltage range of 3.5–4.3 V.

3. Results and discussion

Fig. 1a schematically illustrates the Joule-heating synthesis process of the layered/spinel heterostructured cathode material. The precursor of the cathode material was prepared by using a typical combustion method with a Li/Mn ratio of 1.09:1.91 (see the Experimental Section for details). Excess Li is used for the formation of the layered/spinel heterostructure. Under such condition, non-equilibrium process of Joule-heating occurred in an ultrashort synthesis time, forming Li-rich oxide (Li_2MnO_3) in $LiMn_2O_4$ (LMO). The precursor was then calcined to form the layered/spinel heterostructured cathode material by a two-step Joule heating method, precalcination (~670 ℃ for ~ 9 s) and calcination (~740 ℃ for ~ 9 s) (Fig. S1, Movie S1). During the Joule-heating processe, the ultrafast ramping and quenching rates (10^2–10^3 ℃/s)allow an extremely short synthesis time. This is the fastest synthesis of $LiMn_2O_4$-based cathode materials (Table S1). As a contrast, single-phase LMO was also synthesized using the same calcination conditions with a Li/Mn ratio of 1:2.

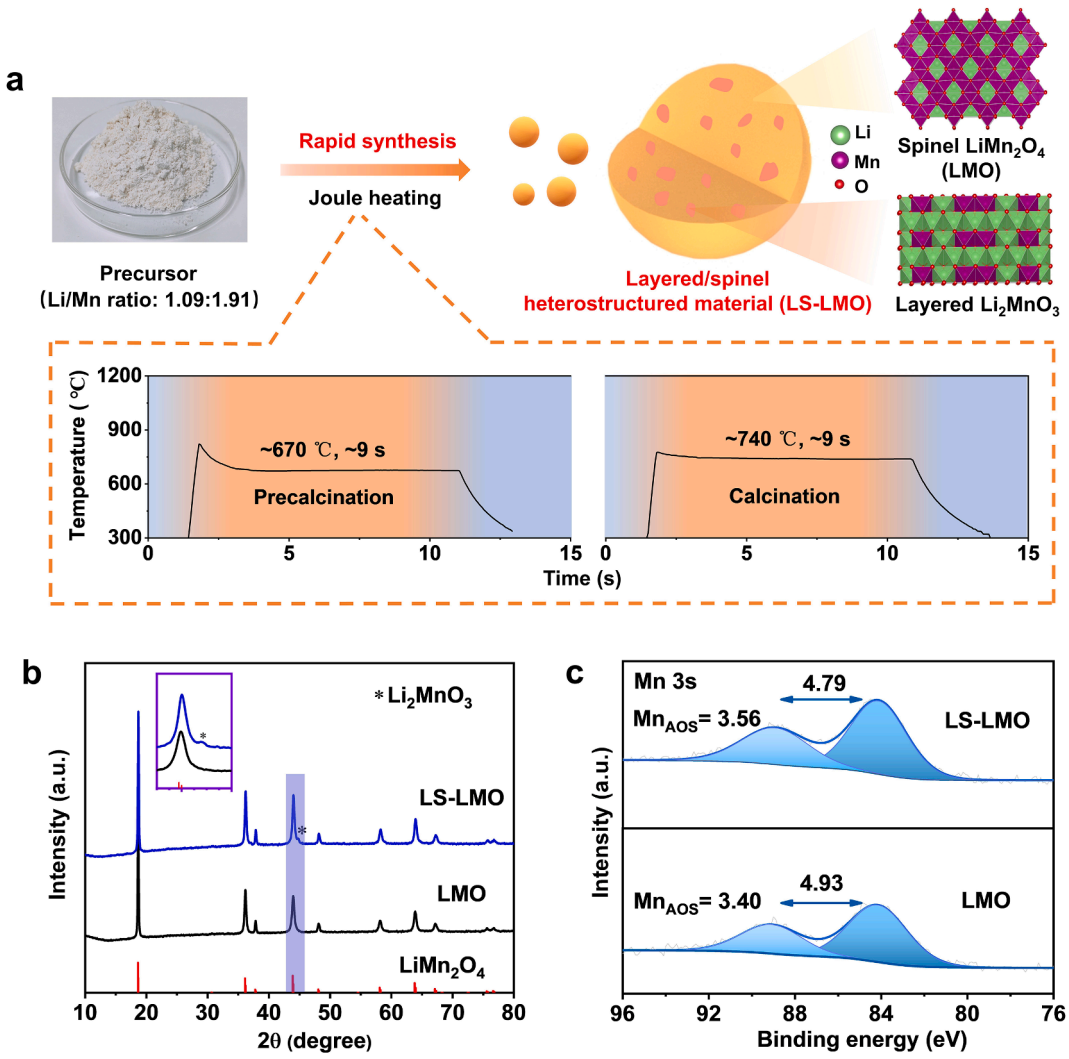

Fig. 1. (a) Schematic of the synthesis of LS-LMO by Joule heating. (b) XRD patterns and (c) XPS spectra of Mn 3 s for LS-LMO and LMO.

The crystal structures of LS-LMO and LMO were investigated by XRD. As displayed in Fig. 1b, the diffraction pattern of LMO is well indexed to a cubic spinel structure with a space group of *Fd-3 m* [23]. The sharp Bragg peaks indicate a good crystallinity. In contrast, a similar diffraction pattern is displayed for LS-LMO, but with new peaks indexed to the layered phase of Li_2MnO_3, indicating that two phases were formed. The phase composition of LS-LMO was investigated by XRD combined with Rietveld refinement (Fig. S2). The results show that LS-LMO consists of 92.8 % spinel phase of $LiMn_2O_4$ and 7.2 % layered phase of Li_2MnO_3. To further analyze the effects of Joule heating on the formation of the heterostructure, the same precursor was calcined using a conventional furnace heat treatment method with a long time heating process. No layered Li_2MnO_3 phase was measured for the product prepared by the conventional method. These results show that the Joule heating process is critical to generate the layered/spinel heterostructure (Fig. S3).

The chemical properties of LS-LMO and LMO were analyzed by XPS (Fig. 1c). The multiplet splitting of Mn 3 s is often used as a sign for the Mn valence [45,46]. For LMO, the valence of Mn is 3.40, lower than the reported values in the literature. This is attributed to the oxygen vacancy produced in the extremely fast synthesis process of Joule heating (Fig. S4) [27,34]. In contrast, the valence of Mn for LS-LMO is 3.56, higher than that of LMO. This should be attributed to the introduction of the layered Li_2MnO_3 phase. The higher Mn valence of LS-LMO can reduce the generation of soluble low-valence Mn ions due to the disproportionation reaction of Mn^{3+}.

The surface morphologies and microstructures of LS-LMO and LMO were investigated by SEM and TEM. A similar morphology of slightly agglomerated particles was displayed, with particle sizes of 50–300 nm, indicating that the introduction of the layered Li_2MnO_3 does not influence the surface morphology (Fig. S5). Similar morphologies are also displayed in the TEM images (Fig. 2a, d), as the observations by SEM. A single cubic spinel phase was clearly characterized for LMO as revealed by the HRTEM and FFT images (Fig. 2b, c). In contrast, in addition to the cubic spinel phase observed for LMO, the layered phase of Li_2MnO_3 is displayed for LS-LMO (Fig. 2e, f). The layered/spinel heterostructure of LS-LMO was further analyzed by aberration-corrected high angle annular dark-field scanning transmission electron microscopy (HAADF-STEM). The atomic arrangements of Mn of the two phases of spinel and layered structures are clearly displayed in the HAADF-STEM image (Fig. 2g). In the layered region, the Mn ion arrangement matches well with the layered phase of Li_2MnO_3. While in the spinel region, the Mn ions are arranged in a diamond pattern, a characteristic of the spinel phase [23]. The atomic arrangements of layered and spinel phases are schematically illustrated in Fig. 2h and i, respectively. There is no disordered structure between these two phases due to the good structural compatibility, referring a good structural stability during cycling. Clearly, the nanoscale heterostructure was successfully synthesized using the ultrafast Joule heating.

The electrochemical performances of LS-LMO and LMO were investigated in coin-type cells using Li metal anodes. Fig. 3a shows the

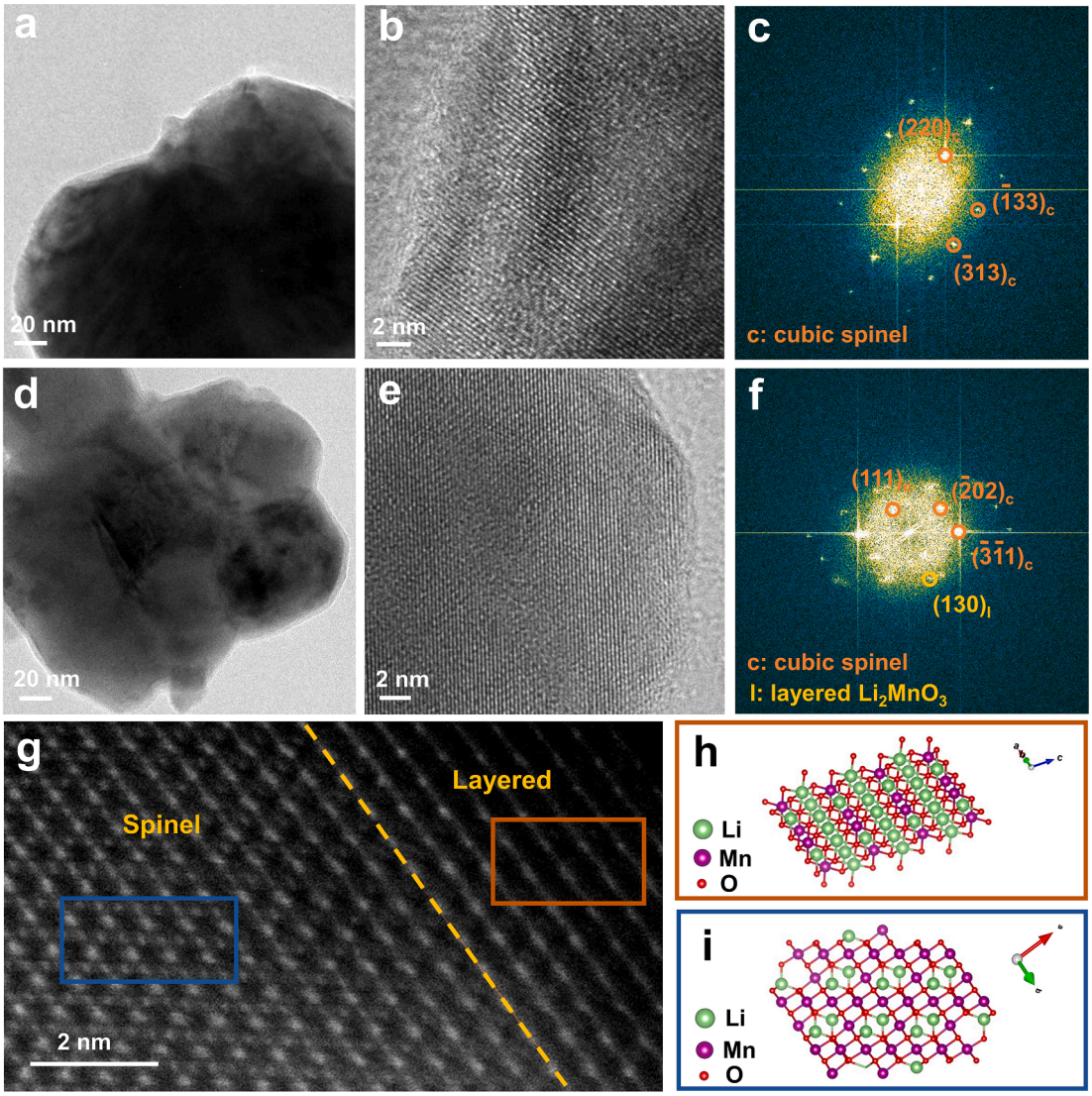

Fig. 2. (a, d) TEM, (b, e) HRTEM, and (c, f) fast Fourier transform images of (a, b, c) LMO and (d, e, f) LS-LMO. (g) The aberration-corrected HAADF-STEM image and atomic structure models of (h) layered and (i) spinel phases of LS-LMO.

galvanostatic charge–discharge profiles in the first cycle at a current rate of 0.1C within 3.5–4.3 V, and Fig. 3b shows the corresponding dQ/dV curves. Typical redox characteristics of $LiMn_2O_4$ are displayed for both LS-LMO and LMO, indicating that the electrochemical behavior of $LiMn_2O_4$ is not influenced by the introduction of the low-content phase of Li_2MnO_3. A higher Coulombic efficiency was obtained for LS-LMO (88.5 %) than LMO (84.6 %), but a similar discharge capacity of ~ 109 mAh g^{-1} was delivered, demonstrating a better reversibility of LS-LMO. The higher Coulombic efficiency of LS-LMO should be attributed to reduced irreversible phase transformation and interfacial side reactions.

The cycling stability of LS-LMO and LMO was evaluated at a current rate of 1C after one-cycle activation at 0.1C (Fig. 3c). After 200 cycles, LS-LMO retained 85 % of its initial capacity, much higher than 72 % of LMO. To verify the practicality of LS-LMO, cycling performance was tested with a high mass loading (~3.0 mg cm^{-2}) at a current rate of 1C after one-cycle activation at 0.1C (Fig. S6). After 200 cycles,a high capacity retention of 84% was obtained. This apparently highlights the advantages of the heterostructure in enhancing the electrochemical performance of the LMO cathode materials. The evolution of the charge–discharge and dQ/dV curves with cycling was investigated and compared (Fig. S7). For LMO, the charge/discharge polarization becomes larger rapidly with cycling, implying a structure degradation. In contrast, LS-LMO shows a negligible voltage polarization change, suggesting a much improved structure stability. This is consistent with the better cycling performance of LS-LMO. The long-term cycling performance of LMO and LS-LMO was evaluated at 5C after 1cycle activation at 0.1C. As shown in Fig. 3d, although the initial capacity of LS-LMO is slightly lower than LMO due to the introduction of electrochemically inert layered Li_2MnO_3 phase, LS-LMO exhibits a drastically improved cycling stability, with 83 % capacity retention versus 62 % of LMO. This is superior to the cycling performance of most LMO cathode materials reported in the literature (Table S2). The superior cycling performance of LS-LMO is ascribed to the unique layered/spinel heterostructure.

To have insights into the structure stability enhancement of LS-LMO, the structural evolution during the charge and discharge processes was investigated by ex-situ XRD (Fig. 4a-d). Except for some peaks indexed to graphite carbon and Al foil, all samples maintain cubic spinel phases throughout the charging process. When discharged from 4.3 to 3.5 V, all samples show an additional tetragonal $Li_{1.5}Mn_{0.97}O_2$ phase. However, the tetragonal phase for LMO is first found at 4.1 V during the discharging process, which is higher than that for LS-LMO (3.5 V), indicating that the cubic-tetragonal phase transformation can be well suppressed by the introduced layered Li_2MnO_3 phase. At the discharge

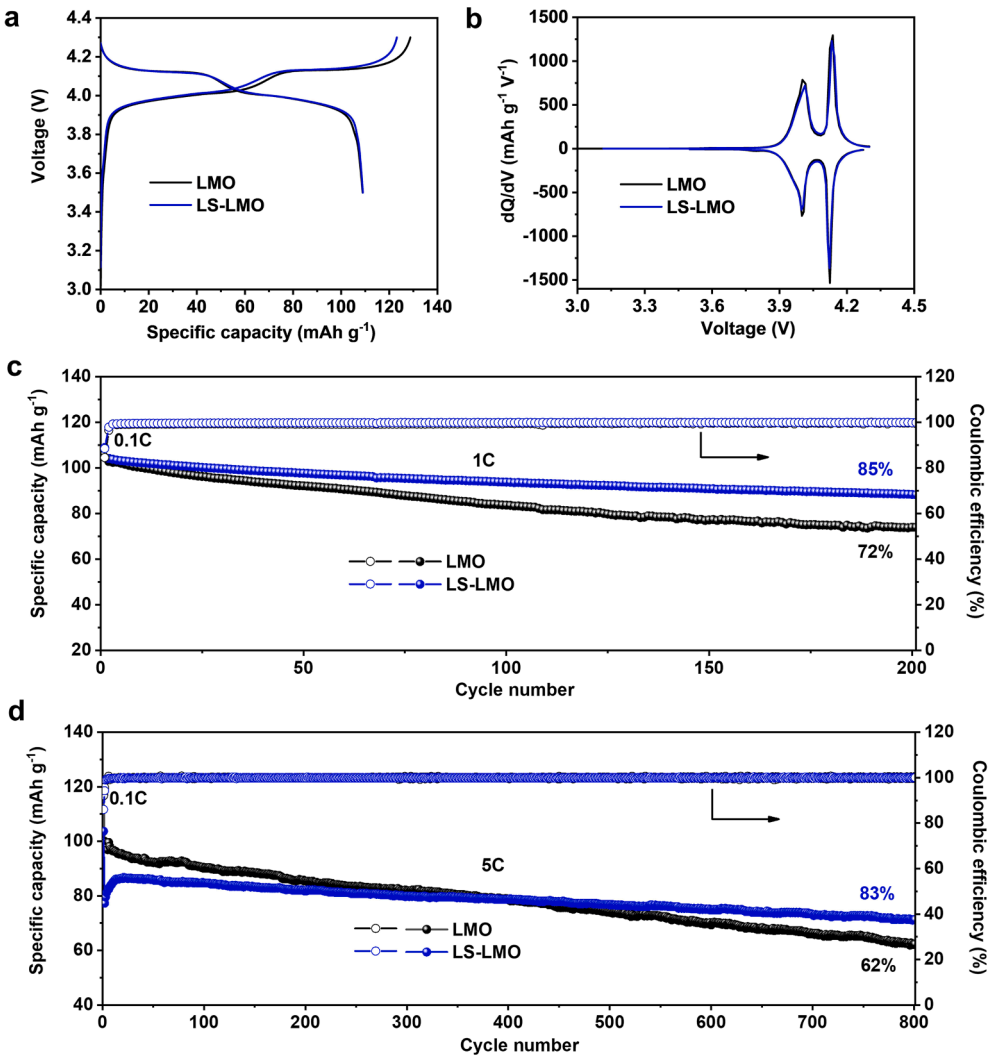

Fig. 3. (a) First charge–discharge curves at 0.1C within 3.5–4.3 V and (b) corresponding dQ/dV curves, (c) cycling performance at 1C and at (d) 5C after one cycle of activation at 0.1C for LS-LMO and LMO.

state of the cubic spinel $LiMn_2O_4$ cathode, the MnO_6 octahedrons undergo an elongation distortion along the dz^2 direction as a result of the Jahn-Teller effect, leading to an irreversible phase transformation from cubic to tetragonal phase (Fig. 5a). The irreversible phase transition not only reduces the specific capacity but also causes a large volume change and structure damage [47–49]. However, for LS-LMO, the introduced layered Li_2MnO_3 phase can act as a retardant, effectively suppressing the elongation distortion of the MnO_6 octahedrons and Jahn-Teller effect (Fig. 5a). Similar phenomena were also reported in other hetero-structured cathode materials [43,50]. To confirm the function of Li_2MnO_3 as a retardant to the Jahn-Teller effect and irreversible phase transformation, the Rietveld refinements of XRD patterns were performed at the discharge state of 3.5 V in the first cycle (Fig. 5b, c). The fraction of the cubic spinel phase is calculated to be 74.4 % for LMO, while 82.7 % for LS-LMO. In addition, as a sign of the Jahn-Teller distortion, the Mn-O bond length in the MnO_6 octahedron is calculated to be 2.059 Å in the dz^2 direction. In contrast, a smaller Mn-O bond length of 2.048 Å in the dz^2 direction is obtained for LS-LMO. This is further verified by the Rietveld refinements of XRD patterns of the cathodes after 100 cycles, 53.8 % cubic spinel phase for LMO vs. 78.4 % for LS-LMO (Figs. S8 and S9).

The reaction kinetics of the LS-LMO and LMO cathodes were investigated by EIS and GITT. The Nyquist plots of LMO and LS-LMO are presented in Fig. 6a and b, respectively. The corresponding equivalent electric circuit is shown in Fig. S10 and the fitting results are listed in Table S3. All Nyquist plots display four parts: the intercept with the horizontal axis at the highest frequency represents the ohmic impedance (R_s); semicircles in the high frequency and middle frequency regions are related to the cathode electrolyte interphase resistance (R_{CEI}) and charge-transfer resistance (R_{ct}), respectively; an oblique line in the low frequency region is related to the Warburg impedance (Z_w) [51]. For LMO, R_{ct} undergoes a continuous increase with cycling, suggesting continuous structural degradation and interface side reactions. In contrast, although LS-LMO exhibits a slightly larger R_{ct} in the first cycle due to the introduction of the inactive layered Li_2MnO_3 phase, a decreased R_{ct} is measured after 100 cycles, demonstrating a stable structure and interface. Furthermore, the GITT results reveal that LS-LMO exhibits lower D_{Li+} values in both charging and discharging processes than LMO, attributed to the introduced layered Li_2MnO_3 phase. This is consistent with EIS results (Figs. S11 and S12).

In addition to the structural degradation, Mn dissolution of the LMO cathodes is also an important factor affecting the electrochemical performance. The Mn dissolution was investigated on the electrodes after 50 and 100 cycles by ICP-OES. Much lower Mn contents were measured for LS-LMO than LMO, 6.7 vs. 10.4 ppb after 50 cycles and 7.8 vs. 12.7 ppb after 100 cycles, indicating that the introduced layered Li_2MnO_3 phase can effectively mitigate the dissolution of Mn (Fig. 6c).

The microstructures and morphologies of the electrodes were

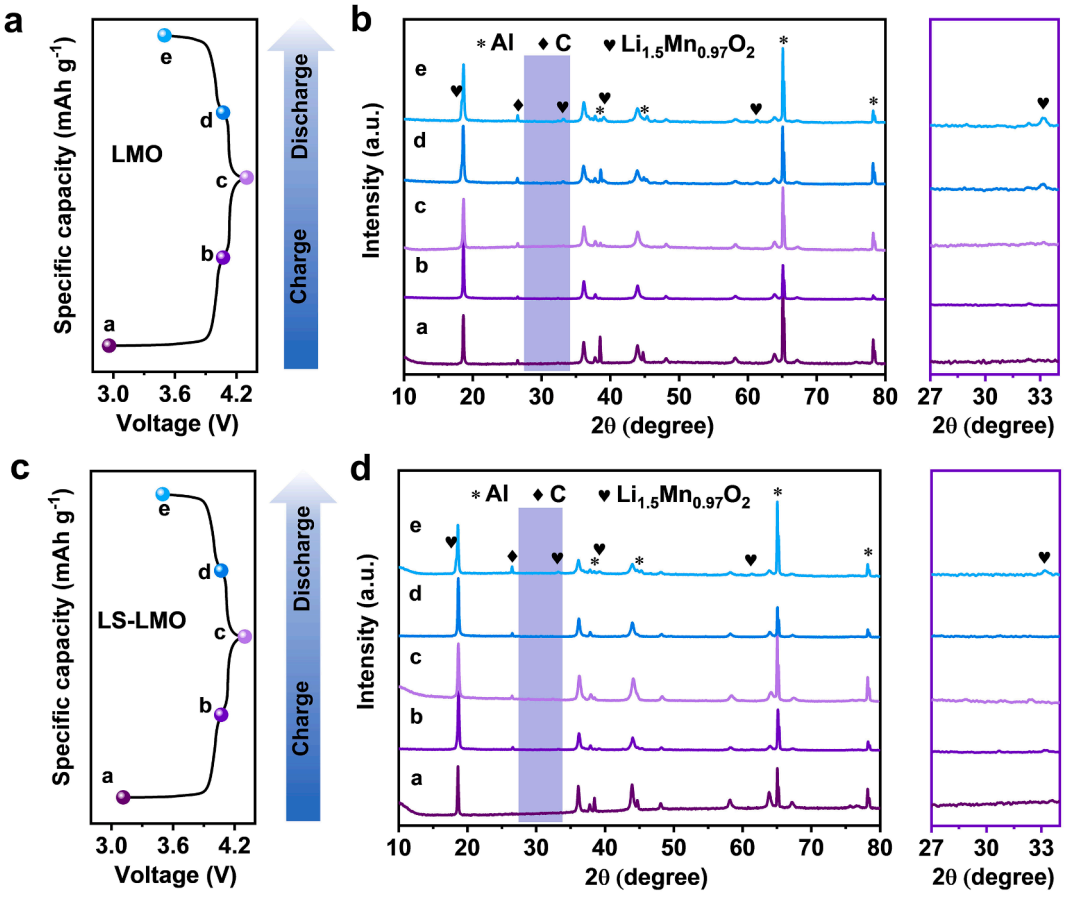

Fig. 4. (a) First charge–discharge curve at 0.1C and (b) corresponding ex-situ XRD patterns for LMO. (c) First charge–discharge curve at 0.1C and (d) corresponding ex-situ XRD patterns for LS-LMO.

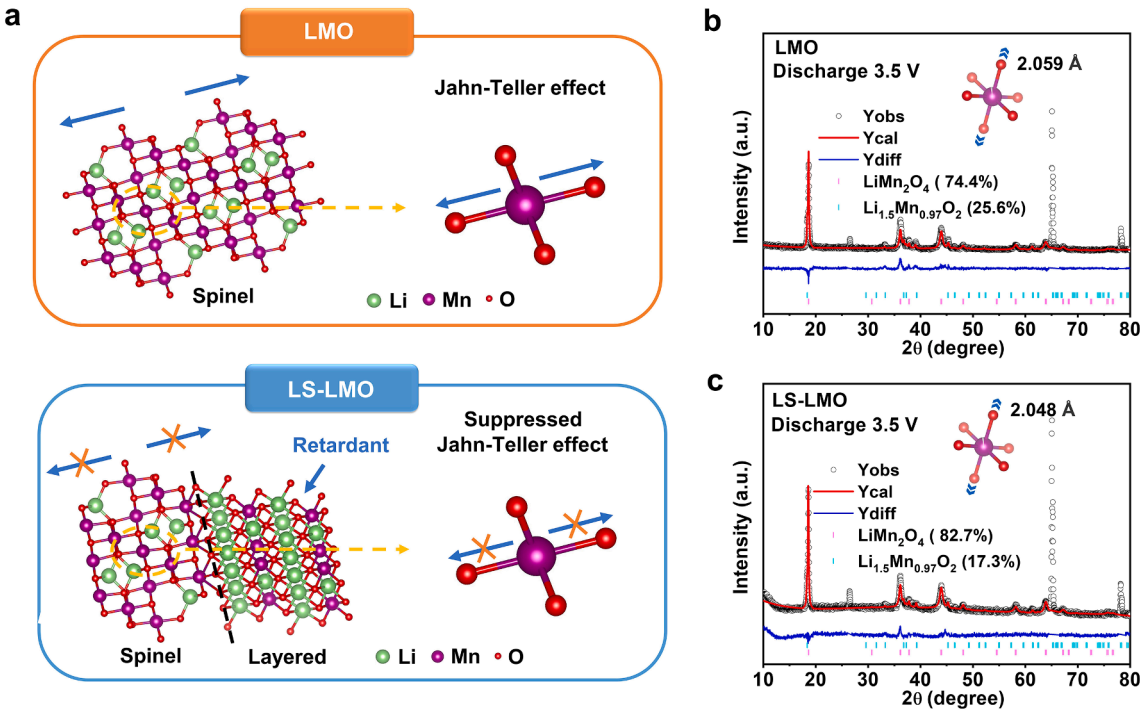

Fig. 5. (a) Schematic diagram to show the introduced layered Li_2MnO_3 phase as a retardant to suppress Jahn-Teller effect. Rietveld-refined XRD patterns of (b) LMO and (c) LS-LMO when discharged to 3.5 V in the first cycle. The insets represent the corresponding MnO_6 octahedra in the tetragonal $Li_{1.5}Mn_{0.97}O_2$ phase.

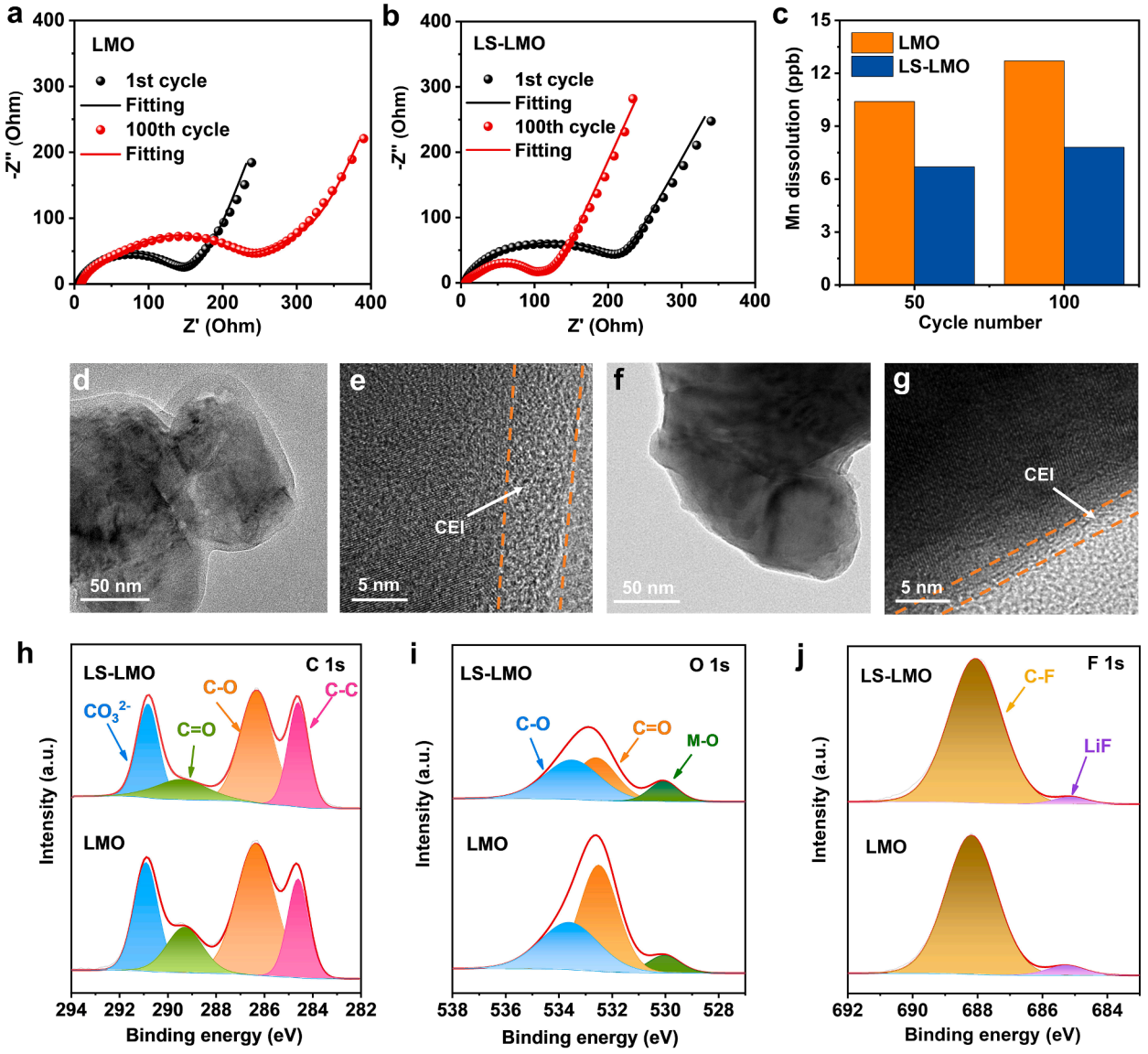

Fig. 6. Nyquist plots after 1 cycle and 100 cycles for (a) LMO and (b) LS-LMO. (c) Mn dissolution of LS-LMO and LMO after 50 cycles and 100 cycles. (d) TEM and (e) HRTEM images of LMO after 100 cycles. (f) TEM and (g) HRTEM images of LS-LMO after 100 cycles. XPS spectra of (h) C 1 s, (i) O 1 s, and (j) F 1 s for LS-LMO and LMO after 100 cycles.

examined by TEM and XPS after 100 cycles. A thick cathode electrolyte interphase (CEI) layer was displayed for LMO (Fig. 6d, e), verifying serious parasitic reactions at the electrode–electrolyte interface. While it is very thin for LS-LMO, implying an effective suppression of the side reactions by the layered Li_2MnO_3 phase on the surface (Fig. 6f, g). The drastic difference was also displayed by the XPS measurements. For LMO, pronounced C-O, C = O, and Li-F peaks are displayed in the C 1 s, O 1 s, and F 1 s spectra, suggesting that a significant amount of organic and inorganic species were produced due to the decomposition of the solvents and lithium salt in the electrolytes [51–53]. In contrast, LS-LMO exhibits weaker C-O/C = O and Li-F peaks, further verifying the suppressed side reactions (Fig. 6h, i, j, Table S4).

4. Conclusion

In summary, a layered/spinel heterostructured cathode material is synthesized in seconds by an ultrafast Joule heating method. An electrochemically-inert layered phase of Li_2MnO_3 is deftly introduced in the spinel phase of $LiMn_2O_4$ to form a heterostructure as a result of the non-equilibrium process produced by the ultrafast Joule heating rate. The layered phase serves as a structure stabilization agent to suppress the structure damage and Mn dissolution, thus promising an improved electrochemical performance, as revealed by the thorough structure characterization and analysis. Our findings provide an efficient design and synthesis strategy for developing low-cost and high-performance cathode materials.

Author contributions

Y. C., Y. X., and W. Z. conceived the concept. W. Z. carried out the experiments. H. S., and J. Z. helped electrochemical analysis. Z. L. created the 3D illustrations. J. Z. conducted the characterization of TEM and STEM. M. L. provided the characterization of SEM. W. Z. wrote paper. Y. C., Y. X., and P. B. revised the paper. All authors discussed the results and commented on the final manuscript.

Conflict of interest

The authors declare no conflict of interest.

Declaration of competing interest

The authors declare that they have no known competing financial interests or personal relationships that could have appeared to influence the work reported in this paper.

Data availability

Data will be made available on request.

Acknowledgements

We acknowledge the financial support of the National Key Research and Development Program of China (Grant No.: 2019YFE0118800).

Appendix A. Supplementary data

Supplementary data to this article can be found online at https://doi.org/10.1016/j.cej.2023.148045.

References

[1] B.C. Melot, J.M. Tarascon, Design and preparation of materials for advanced electrochemical storage, Acc. Chem. Res. 46 (2013) 1226–1238, https://doi.org/10.1021/ar300088q.
[2] J.B. Goodenough, K.S. Park, The Li-ion rechargeable battery: a perspective, J. Am. Chem. Soc. 135 (2013) 1167–1176, https://doi.org/10.1021/ja3091438.
[3] K.J. Griffith, K.M. Wiaderek, G. Cibin, L.E. Marbella, C.P. Grey, Niobium tungsten oxides for high-rate lithium-ion energy storage, Nature 559 (2018) 556–563, https://doi.org/10.1038/s41586-018-0347-0.
[4] J. Lee, D.A. Kitchaev, D.H. Kwon, C.W. Lee, J.K. Papp, Y.S. Liu, Z.Y. Lun, R. J. Clement, T. Shi, B.D. McCloskey, J.H. Guo, M. Balasubramanian, G. Ceder, Reversible Mn2+/Mn4+ double redox in lithium-excess cathode materials, Nature 556 (2018) 185–190, https://doi.org/10.1038/s41586-018-0015-4.
[5] C. Zhan, T.P. Wu, J. Lu, K. Amine, Dissolution, migration, and deposition of transition metal ions in Li-ion batteries exemplified by Mn-based cathodes - a critical review, Energy Environ. Sci. 11 (2018) 243–257, https://doi.org/10.1039/c7ee03122j.
[6] W.J. Zhang, Structure and performance of $LiFePO_4$ cathode materials: A review, J. Power Sources 196 (2011) 2962–2970, https://doi.org/10.1016/j.jpowsour.2010.11.113.
[7] Y.C. Lyu, X. Wu, K. Wang, Z.J. Feng, T. Cheng, Y. Liu, M. Wang, R.M. Chen, L. M. Xu, J.J. Zhou, Y.H. Lu, B.K. Guo, An Overview on the Advances of LiCoO(2) Cathodes for Lithium-Ion Batteries, Adv. Energy Mater. 11 (2021) 2000982, https://doi.org/10.1002/aenm.202000982.
[8] J. Kim, H. Lee, H. Cha, M. Yoon, M. Park, J. Cho, Prospect and Reality of Ni-Rich Cathode for Commercialization, Adv. Energy Mater. 8 (2018) 1702028, https://doi.org/10.1002/aenm.201702028.
[9] Y.K. Lei, J. Ni, Z.J. Hu, Z.M. Wang, F.K. Gui, B. Li, P.W. Ming, C.M. Zhang, Y. Elias, D. Aurbach, Q.F. Xiao, Surface Modification of Li-Rich Mn-Based Layered Oxide Cathodes: Challenges, Materials, Methods, and Characterization, Adv. Energy Mater. 10 (2020) 2002506, https://doi.org/10.1002/aenm.202002506.
[10] S.H. Li, H.X. Li, H.Y. Zhang, S. Zhang, Y.Q. Lai, Z. Zhang, Constructing stable surface structures enabling fast charging for Li-rich layered oxide cathodes, Chem. Eng. J. 427 (2022), 132036, https://doi.org/10.1016/j.cej.2021.132036.
[11] O.K. Park, Y. Cho, S. Lee, H.C. Yoo, H.K. Song, J. Cho, Who will drive electric vehicles, olivine or spinel? Energy Environ. Sci. 4 (2011) 1621–1633, https://doi.org/10.1039/c0ee00559b.
[12] W. Huang, G. Wang, C. Luo, Y.B. Xu, Y. Xu, B.J. Eckstein, Y. Chen, B.H. Wang, J. X. Huang, Y.J. Kang, J.S. Wu, V.P. Dravid, A. Facchetti, T.J. Marks, Controllable growth of $LiMn_2O_4$ by carbohydrate-assisted combustion synthesis for high performance Li-ion batteries, Nano Energy 64 (2019), 103936, https://doi.org/10.1016/j.nanoen.2019.103936.
[13] A.K. Shukla, T.P. Kumar, Nanostructured electrode materials for electrochemical energy storage and conversion, Wiley Interdiscipl. Rev. Energy Environ. 2 (2013) 14–30, https://doi.org/10.1002/wene.48.
[14] J. Abou-Rjeily, I. Bezza, N.A. Laziz, C. Autret-Lambert, M.T. Sougrati, F. Ghamouss, High-rate cyclability and stability of $LiMn_2O_4$ cathode materials for lithium-ion batteries from low-cost natural beta-MnO_2, Energy Storage Mater. 26 (2020) 423–432, https://doi.org/10.1016/j.ensm.2019.11.015.
[15] A.H. Marincas, F. Goga, S.A. Dorneanu, P. Ilea, Review on synthesis methods to obtain $LiMn_2O_4$-based cathode materials for Li-ion batteries, J. Solid State Electrochem. 24 (2020) 473–497, https://doi.org/10.1007/s10008-019-04467-3.
[16] X.N. Wang, X.Y. Chen, L.H. Gao, H.G. Zheng, M.R. Ji, T. Shen, Z.D. Zhang, Citric acid-assisted sol-gel synthesis of nanocrystalline $LiMn_2O_4$ spinel as cathode material, J. Cryst. Growth 256 (2003) 123–127, https://doi.org/10.1016/s0022-0248(03)01289-2.
[17] G.G. Wang, J.M. Wang, W.Q. Mao, H.B. Shao, J.Q. Zhang, C.N. Cao, Physical properties and electrochemical performance of $LiMn_2O_4$ cathode materials prepared by a precipitation method, J. Solid State Electrochem. 9 (2005) 524–530, https://doi.org/10.1007/s10008-004-0607-9.
[18] D. Ahn, M. Song, Variations of the electrochemical properties of $LiMn_2O_4$ with synthesis conditions, J. Electrochem. Soc. 147 (2000) 874–879, https://doi.org/10.1149/1.1393285.
[19] P. Angelopoulou, F. Paloukis, G. Slowik, G. Wojcik, G. Avgouropoulos, Combustion-synthesized $Li_xMn_2O_4$-based spinel nanorods as cathode materials for lithium-ion batteries, Chem. Eng. J. 311 (2017) 191–202, https://doi.org/10.1016/j.cej.2016.11.082.
[20] M. Nakayama, K. Watanabe, H. Ikuta, Y. Uchimoto, M. Wakihara, Grain size control of $LiMn_2O_4$ cathode material using microwave synthesis method, Solid State Ionics 164 (2003) 35–42, https://doi.org/10.1016/j.ssi.2003.08.048.
[21] Y. Terada, Y. Nishiwaki, I. Nakai, F. Nishikawa, Study of Mn dissolution from $LiMn_2O_4$ spinel electrodes using in situ total reflection X-ray fluorescence analysis and fluorescence XAFS technique, J. Power Sources 97–8 (2001) 420–422, https://doi.org/10.1016/s0378-7753(01)00741-8.
[22] D.C. Tang, Y. Sun, Z.Z. Yang, L.B. Ben, L. Gu, X.J. Huang, Surface Structure Evolution of $LiMn_2O_4$ Cathode Material upon Charge/Discharge, Chem. Mater. 26 (2014) 3535–3543, https://doi.org/10.1021/cm501125e.
[23] C.D. Amos, M.A. Roldan, M. Varela, J.B. Goodenough, P.J. Ferreira, Revealing the Reconstructed Surface of Li Mn-2 O-4, Nano Lett. 16 (2016) 2899–2906, https://doi.org/10.1021/acs.nanolett.5b03926.
[24] Y.M. Huang, Y.H. Dong, S. Li, J. Lee, C. Wang, Z. Zhu, W.J. Xue, Y. Li, J. Li, Lithium Manganese Spinel Cathodes for Lithium-Ion Batteries, Adv. Energy Mater. 11 (2021) 2000997, https://doi.org/10.1002/aenm.202000997.
[25] Z.F. Cai, Y.Z. Ma, X.N. Huang, X.H. Yan, Z.X. Yu, S.H. Zhang, G.S. Song, Y.L. Xu, C. E. Wen, W.D. Yang, High electrochemical stability Al-doped spinel $LiMn_2O_4$ cathode material for Li-ion batteries, J. Energy Storage 27 (2020), 101036, https://doi.org/10.1016/j.est.2019.101036.
[26] R.J. Gummow, A.D. Kock, M.M. Thackeray, Improved capacity retention in rechargeable 4 V lithium/lithium-manganese oxide (spinel) cells, Solid State Ionics 69 (1994) 59–67.
[27] Y.Z. Duan, J.M. Guo, M.W. Xiang, J.Y. Zhu, C.W. Su, H.L. Bai, X.F. Liu, W. Bai, R. Wang, Single crystalline polyhedral $LiNi_xMn_{2-x}O_4$ as high-performance cathodes for ultralong cycling lithium-ion batteries, Solid State Ionics 326 (2018) 100–109, https://doi.org/10.1016/j.ssi.2018.09.014.
[28] M.W. Xiang, C.W. Su, L.L. Feng, M.L. Yuan, J.M. Guo, Rapid synthesis of high-cycling performance LiMgxMn2-xO4 (x <= 0.20) cathode materials by a low-temperature solid-state combustion method, Electrochim. Acta 125 (2014) 524–529, https://doi.org/10.1016/j.electacta.2014.01.147.
[29] W.K. Kim, D.W. Han, W.H. Ryu, S.J. Lim, H.S. Kwon, Al_2O_3 coating on $LiMn_2O_4$ by electrostatic attraction forces and its effects on the high temperature cyclic performance, Electrochim. Acta 71 (2012) 17–21, https://doi.org/10.1016/j.electacta.2012.03.090.
[30] J.Q. Zhao, Y. Wang, Ultrathin Surface Coatings for Improved Electrochemical Performance of Lithium Ion Battery Electrodes at Elevated Temperature, J. Phys. Chem. C 116 (2012) 11867–11876, https://doi.org/10.1021/jp3010629.
[31] Y.H. Shang, X.J. Lin, X. Lu, T. Huang, A.H. Yu, Nano-TiO2(B) coated LiMn2O4 as cathode materials for lithium-ion batteries at elevated temperatures, Electrochim. Acta 156 (2015) 121–126, https://doi.org/10.1016/j.electacta.2015.01.024.
[32] D.Q. Liu, Z.Z. He, X. Liu, Increased cycling stability of $AlPO_4$-coated $LiMn_2O_4$ for lithium ion batteries, Mater. Lett. 61 (2007) 4703–4706, https://doi.org/10.1016/j.matlet.2007.03.012.
[33] P. Mohan, G.P. Kalaignan, Structure and electrochemical performance of surface modified $LaPO_4$ coated $LiMn_2O_4$ cathode materials for rechargeable lithium batteries, Ceram. Int. 40 (2014) 1415–1421, https://doi.org/10.1016/j.ceramint.2013.07.024.
[34] M. Jeong, M.J. Lee, J. Cho, S. Lee, Surface Mn Oxidation State Controlled Spinel $LiMn_2O_4$ as a Cathode Material for High-Energy Li-Ion Batteries, Adv. Energy Mater. 5 (2015) 1500440, https://doi.org/10.1002/aenm.201500440.
[35] L. Chen, R.E. Warburton, K.S. Chen, J.A. Libera, C. Johnson, Z.Z. Yang, M. C. Hersam, J.P. Greeley, J.W. Elam, Mechanism for Al_2O_3 Atomic Layer Deposition on $LiMn_2O_4$ from In Situ Measurements and Ab Initio Calculations, Chem. 4 (2018) 2418–2435, https://doi.org/10.1016/j.chempr.2018.08.006.
[36] Y.L. Ding, J.A. Xie, G.S. Cao, T.J. Zhu, H.M. Yu, X.B. Zhao, Single-Crystalline $LiMn_2O_4$ Nanotubes Synthesized Via Template-Engaged Reaction as Cathodes for High-Power Lithium Ion Batteries, Adv. Funct. Mater. 21 (2011) 348–355, https://doi.org/10.1002/adfm.201001448.
[37] D.K. Kim, P. Muralidharan, H.W. Lee, R. Ruffo, Y. Yang, C.K. Chan, H. Peng, R. A. Huggins, Y. Cui, Spinel $LiMn_2O_4$ Nanorods as Lithium Ion Battery Cathodes, Nano Lett. 8 (2008) 3948–3952, https://doi.org/10.1021/nl8024328.
[38] Y.N. Chen, G.C. Egan, J.Y. Wan, S.Z. Zhu, R.J. Jacob, W.B. Zhou, J.Q. Dai, Y. B. Wang, V.A. Danner, Y.G. Yao, K. Fu, Y.B. Wang, W.Z. Bao, T. Li, M.R. Zachariah, L.B. Hu, Ultra-fast self-assembly and stabilization of reactive nanoparticles in reduced graphene oxide films, Nat. Commun. 7 (2016) 12332, https://doi.org/10.1038/ncomms12332.
[39] C.W. Wang, W.W. Ping, Q. Bai, H.C. Cui, R. Hensleigh, R.L. Wang, A.H. Brozena, Z. P. Xu, J.Q. Dai, Y. Pei, C.L. Zheng, G. Pastel, J.L. Gao, X.Z. Wang, H. Wang, J. C. Zhao, B. Yang, X.Y. Zheng, J. Luo, Y.F. Mo, B. Dunn, L.B. Hu, A general method

to synthesize and sinter bulk ceramics in seconds, Science 368 (2020) 521–526, https://doi.org/10.1126/science.aaz7681.
[40] S.L. Liu, Y. Shen, Y. Zhang, B.H. Cui, S.B. Xi, J.F. Zhang, L.Y. Xu, S.Z. Zhu, Y. A. Chen, Y.D. Deng, W.B. Hu, Extreme Environmental Thermal Shock Induced Dislocation-Rich Pt Nanoparticles Boosting Hydrogen Evolution Reaction, Adv. Mater. 34 (2022) 2106973, https://doi.org/10.1002/adma.202106973.
[41] W. Zhu, J.C. Zhang, J.W. Luo, C.H. Zeng, H. Su, J.F. Zhang, R. Liu, E.Y. Hu, Y. S. Liu, W.D. Liu, Y.A. Chen, W.B. Hu, Y.H. Xu, Ultrafast Non-Equilibrium Synthesis of Cathode Materials for Li-Ion Batteries, Adv. Mater. 35 (2023) 2208974, https://doi.org/10.1002/adma.202208974.
[42] T.Y. Li, Y.G. Yao, Z.N. Huang, P.F. Xie, Z.Y. Liu, M.H. Yang, J.L. Gao, K.Z. Zeng, A. H. Brozena, G. Pastel, M.L. Jiao, Q. Dong, J.Q. Dai, S.K. Li, H. Zong, M.F. Chi, J. Luo, Y.F. Mo, G.F. Wang, C. Wang, R. Shahbazian-Yassar, L.B. Hu, Denary oxide nanoparticles as highly stable catalysts for methane combustion, Nat. Catal. 4 (2021) 62–70, https://doi.org/10.1038/s41929-020-00554-1.
[43] L.G. Wang, T.C. Liu, T.P. Wu, J. Lu, Strain-retardant coherent perovskite phase stabilized Ni-rich cathode, Nature 611 (2022) 61–67, https://doi.org/10.1038/s41586-022-05238-3.
[44] B.H. Toby, EXPGUI, a graphical user interface for GSAS, J. Appl. Crystallogr. 34 (2001) 210–213, https://doi.org/10.1107/s0021889801002242.
[45] X.K. Ding, D. Luo, J.X. Cui, H.X. Xie, Q.Q. Ren, Z. Lin, An Ultra-Long-Life Lithium-Rich $Li_{1.2}Mn_{0.6}Ni_{0.2}O_2$ Cathode by Three-in-One Surface Modification for Lithium-Ion Batteries, Angew. Chem. Int. Ed. 59 (2020) 7778–7782, https://doi.org/10.1002/anie.202000628.
[46] A. Li, C.F. Li, P.X. Xiong, J.F. Zhang, D.L. Geng, Y.H. Xu, Rapid synthesis of layered K_xMnO_2 cathodes from metal-organic frameworks for potassium-ion batteries, Chem. Sci. 13 (2022) 7575–7580, https://doi.org/10.1039/d2sc02442j.
[47] A. Yamada, M. Tanaka, K. Tanaka, K. Sekai, Jahn-Teller instability in spinel Li-Mn-O, J. Power Sources 81 (1999) 73–78, https://doi.org/10.1016/s0378-7753(99)00106-8.
[48] M.M. Thackeray, Y. Shao-Horn, A.J. Kahaian, K.D. Kepler, J.T. Vaughey, S. A. Hackney, Structural fatigue in spinel electrodes in high voltage (4V) Li/LixMn2O4 cells, Electrochem. Solid State Lett. 1 (1998) 7–9.
[49] C.Y. Ouyang, S.Q. Shi, M.S. Lei, Jahn-Teller distortion and electronic structure of $LiMn_2O_4$, J. Alloys Compd. 474 (2009) 370–374, https://doi.org/10.1016/j.jallcom.2008.06.123.
[50] B. Li, G. Rousse, L.T. Zhang, M. Avdeev, M. Deschamps, A.M. Abakumov, J. M. Tarascon, Constructing "Li-rich Ni-rich" oxide cathodes for high-energy-density Li-ion batteries, Energy Environ. Sci. 16 (2023) 1210–1222, https://doi.org/10.1039/d2ee03969a.
[51] G.G. Zhang, M. Chen, C.X. Li, B.H. Wu, J.K. Chen, W.J. Xiang, X.Y. Wen, D. H. Zhang, G.Z. Cao, W.S. Li, Surface spinel and interface oxygen vacancies enhanced lithium-rich layered oxides with excellent electrochemical performances, Chem. Eng. J. 443 (2022), 136434, https://doi.org/10.1016/j.cej.2022.136434.
[52] J.M. Zheng, M.H. Engelhard, D.H. Mei, S.H. Jiao, B.J. Polzin, J.G. Zhang, W. Xu, Electrolyte additive enabled fast charging and stable cycling lithium metal batteries, Nat. Energy 2 (2017) 17012, https://doi.org/10.1038/nenergy.2017.12.
[53] L.L. Wang, J. Ma, C. Wang, X.R. Yu, R. Liu, F. Jiang, X.W. Sun, A.B. Du, X.H. Zhou, G.L. Cui, A Novel Bifunctional Self-Stabilized Strategy Enabling 4.6 V $LiCoO_2$ with Excellent Long-Term Cyclability and High-Rate Capability, Adv. Sci. 6 (2019) 1900355, https://doi.org/10.1002/advs.201900355.